

# Point-localized, site-specific membrane potential optical recording by single fluorescent nanodiscs

Asaf Grupi,<sup>1,2,\*</sup> Zehavit Shapira,<sup>1,2</sup> Shimon Yudovich,<sup>1,2</sup> Nurit Degani-Katzav,<sup>1,2</sup> and Shimon Weiss<sup>1,2,3,4,\*</sup>

<sup>1</sup>Department of Physics, Institute for Nanotechnology and Advanced Materials and <sup>2</sup>Institute for Nanotechnology and Advanced Materials, Bar-Ilan University, Ramat-Gan, Israel; and <sup>3</sup>Department of Chemistry and Biochemistry and <sup>4</sup>California NanoSystems Institute, University of California Los Angeles, Los Angeles, California

**ABSTRACT** Nanodisc technology was implemented as a platform for voltage nanosensors. A fluorescence (Förster) resonance energy transfer (FRET)-based voltage-sensing scheme employing fluorescent nanodiscs and the hydrophobic ion dipyrilamine was developed and utilized to optically record membrane potentials on the single-nanodisc level. Ensemble and single-nanosensor recordings were demonstrated for HEK293 cells and primary cortical neuron cells. Conjugation of nanodiscs to anti-GABA<sub>A</sub> antibodies allowed for site-specific membrane potential measurements from postsynaptic sites.

**WHY IT MATTERS** We developed nanotechnology-based sensors (using lipid nanodisc technology) that can record membrane potentials on the nanoscale. These nanosensors can be targeted and record electrophysiological signals from individual synapses.

## INTRODUCTION

Functional states of brain activity result from the correlated action of a large ensemble of neurons. With each neuron forming synaptic contacts with thousands of other neurons, the function of a neural circuit is an emergent property of these interactions, unpredictable by analysis of the functional properties of individual neurons (1). Although multielectrode recordings have provided important insights from single (or a small number of) neurons, they showed limited performance in analyzing dense local circuits or when signals from specific types of nearby neurons need to be distinguished. Moreover, membrane potentials are not uniform in time and space across the membrane of a single neuron and are likely to contribute to emergent properties of large neuronal systems (2). An understanding of the functional properties of neural circuits requires dynamic recording of membrane potentials (and action potentials) from every neuron and its subcellular components.

For this reason, considerable efforts have been invested in developing optical recording methods that allow for simultaneous direct visualization of neuronal activity over a large number of neurons in a large field of view. Voltage-sensitive dyes (VSDs) (3,4) and genetically encoded voltage indicators (GEVIs) (5–7) are being used for neuroimaging at the ensemble level and in both *in vitro* and *in vivo* formats. Although synthetic VSDs are typically superior to GEVIs in terms of photostability, brightness, and voltage sensitivity (8–10), GEVIs allow for genetic targeting to specific cell types, providing a valuable experimental tool for the study of complex neural circuits (11,12). To benefit from both approaches, hybrid indicators were developed by combining small-molecule fluorophores and genetically encoded proteins (13–15). Apart from the cytoplasmic membrane, other subcellular membranes such as the mitochondria, endoplasmic reticulum, and lysosomes were investigated using these novel tools, utilizing dyes (16), GEVIs (17), or membrane-bound fluorescent donors coupled to a nonfluorescent voltage-dependent acceptor (18).

However, the potential for neuroimaging by VSDs and GEVIs is not fully exploited because of shortcomings such as alteration of membrane capacitance, phototoxicity, and photobleaching (19). More importantly, they do not allow for localized, site-specific membrane potential measurements.

Submitted April 26, 2021, and accepted for publication July 20, 2021.

\*Correspondence: [grupia@gmail.com](mailto:grupia@gmail.com) or [sweiss@chem.ucla.edu](mailto:sweiss@chem.ucla.edu)

Asaf Grupi, Zehavit Shapira, and Shimon Yudovich contributed equally to this work.

Editor: Hagen Hofmann.

<https://doi.org/10.1016/j.bpr.2021.100007>

© 2021 The Author(s).

This is an open access article under the CC BY-NC-ND license (<http://creativecommons.org/licenses/by-nc-nd/4.0/>).



Recently, voltage-sensing nanoparticles (vsNPs) have been developed for noninvasive optical recording of membrane potential at the single-particle and nanoscale level, at multiple sites, in a large field of view (20,21). In contrast to VSDs and GEVIs, vsNPs allow for nanoscale, single-particle voltage detection. However, vsNPs still face challenges associated with functionalization, bioconjugation, stable membrane insertion, toxicity, and uniformity. For these reasons, the development of nontoxic and biodegradable voltage nanosensors would be highly advantageous.

Advances in the field of structural biology of membrane proteins have yielded nanodisc (ND) technology (22). This technology is based on the self-assembly of engineered variants of apolipoprotein A and phospholipids into discoidal nanoparticles. Nanodiscs are relatively easy to produce, are composed of biological macromolecules and therefore biodegradable and nontoxic, can be modified and functionalized via their lipid headgroups or the protein side chains, and are capable of incorporating various types of lipids and lipophilic additives.

We identified NDs as a potential system for local membrane potential nanosensors by an established fluorescence (Förster) resonance energy transfer (FRET)-based sensing mechanism (23). We hypothesized that by incorporating several lipophilic (donor) dyes into a single ND and attaching it to a cell membrane, FRET-based sensing of membrane potential could be achieved between the dyes in the ND and the nonfluorescent lipophilic ion dipicrylamine (DPA), which functions as a FRET acceptor. DPA partitioning between the inner and outer leaflet in response to membrane depolarization leads to membrane potential dependent FRET changes.

Exploratory testing of the utility of such NDs revealed complete quenching of donor dyes by the water-soluble fraction of DPA. This was resolved by incorporation of an additional fluorescent acceptor to the ND bilayer to provide a competing route for energy transfer and using avidin as a steric barrier between the labeled NDs and the surrounding DPA molecules.

The performance of NDs as membrane potential sensors was tested and characterized by electrophysiology experiments conducted on human embryonic kidney (HEK) 293 cells and primary cortical neurons, as well as site-specific membrane potential measurements by antibody-conjugated NDs. Outlook of the technology and future developments are briefly discussed.

## MATERIALS AND METHODS

### Materials

1,2-dimyristoyl-sn-glycero-3-phosphocholine (DMPC), 1,2-dioleoyl-sn-glycero-3-phosphoethanolamine-N-(TopFluor® AF488) (TF), 1,2-di-

palmitoyl-sn-glycero-3-phosphoethanolamine-N-(biotinyl) (biotinyl-PE), 1,2-dioleoyl-sn-glycero-3-phosphoethanolamine-N-(Cyanine 5) (Cy5-PE), and 3 $\beta$ -[N-(N',N'-dimethylaminoethane)-carbonyl] (DC)-cholesterol were purchased from Avanti Polar Lipids (Alabaster, AL). Anti-GABA<sub>A</sub> receptor  $\gamma$ 2 IgG (cat#: 224004) was purchased from Synaptic Systems (Göttingen, Germany). Antibody azido modification click (SiteClick, ThermoFisher) was purchased from Thermo Fisher Scientific (Waltham, MA). All other materials were purchased from Sigma-Aldrich (St. Louis, MO) at the appropriate purity level.

### Plasmid extraction and purification

pMSP1E3D1 (Addgene plasmid #20066; <http://www.addgene.org/20066/>; Research Resource Identifier (RRID) :Addgene\_20066) and pMSP1E3D1\_D73C plasmids (Addgene plasmid #39328; <http://www.addgene.org/39328/>; RRID:Addgene\_39328) were a gift from Stephen Sligar. Plasmids in a bacterial stab were isolated by streaking bacteria onto an agar plate containing 50 mg/mL kanamycin, followed by overnight incubation at 37°C and selection of a single colony for overnight inoculation in 10 mL of Luria broth (LB) / kanamycin at 37°C. Cells were harvested by centrifugation at 6000  $\times$  g for 10 min, and the pellet was resuspended in LB/kanamycin for plasmid extraction and purification using a GenElute plasmid miniprep kit (Sigma-Aldrich).

The purified plasmid was transformed into BL21(DE3) *Escherichia coli* that were subsequently streak onto agar plates containing 50 mg/mL kanamycin. Single colonies isolated from the LB-agar/kanamycin plates were inoculated for 6 h at 37°C, harvested by centrifugation at 6000  $\times$  g for 10 min, and resuspended with fresh LB/kanamycin. The suspension was diluted 1:1 with glycerol to a final 50%, mixed and dispensed to aliquots, and stored in  $-80^{\circ}\text{C}$ .

### MSP expression

BL21(DE3) bacteria transformed with MSP1E3D1 or MSP1E3D1\_D73C plasmids were slowly thawed on ice, and 50  $\mu\text{L}$  of the thawed bacteria was transferred to 10 mL LB containing 50 mg/mL kanamycin. The suspension was inoculated at 37°C with shaking at 220 RPM until an OD<sub>600</sub> of 0.8–1 was reached. The cell suspension was centrifuged at 6000  $\times$  g for 10 min, and the pellet was resuspended in 10 mL of fresh LB/kanamycin solution. 5 mL of the suspension were transferred to 500 mL of EZbroth/kanamycin in a 2 L flask for shaking at 37°C, 220 RPM until an OD of 2.5 was reached. Then, 500  $\mu\text{L}$  of a freshly prepared 1 M isopropyl  $\beta$ -D-thiogalactoside (IPTG) stock was added to the cell suspension to a final 1 mM IPTG for initiation of protein expression. Cell culture was further incubated at 37°C for 4 h. Cells were harvested by centrifugation at 6000  $\times$  g for 10 min. Cell pellet was collected and stored in  $-80^{\circ}\text{C}$ .

### MSP purification

In a typical preparation,  $\sim 10$  g of cell pellet was thawed on ice and resuspended in 90 mL phosphate-buffered saline (PBS). After complete resuspension, 10 mL of 10% Triton X-100 was added to a final 1% concentration with stirring. Deoxyribonuclease was added to a final 2.5  $\mu\text{g}/\text{mL}$ , and the solution was left to stir for 20 min on ice. Cells were lysed by probe sonication using a 3 mm probe (VCX 130; Sonics, Newton, CT) for three 1 min rounds at 40% intensity or until the suspension changed color to dark brown. The suspension was centrifuged at 11,000  $\times$  g for 45 min in 50 mL polystyrene centrifuge tubes to remove cell debris and was subsequently filtered by a 0.22  $\mu\text{m}$  PES syringe filter.

The solution was loaded on an Ni-NTA column pre-equilibrated with 40 mM PBS buffer. Column outlet was connected to a quartz flow cell (0.1 mm pathlength; Hellma, Müllheim, Germany). UV absorbance of

the elution volume was monitored at 280 nm by an Ocean Optics USB4000 spectrophotometer (Ostfildern, Germany). The column was washed with 100 mL of each of the following: 1) 40 mM Tris/HCl, 300 mM NaCl, 1% Triton X-100 (pH 8); 2) 40 mM Tris/HCl, 300 mM NaCl, 50 mM sodium cholate, 20 mM imidazole (pH 8); and 3) 40 mM Tris/HCl, 300 mM NaCl, 50 mM imidazole (pH 8). Finally, MSP was eluted by column wash with 40 mM Tris/HCl, 300 mM NaCl, 400 mM imidazole (pH 8). MSP-containing fractions were dialyzed against 20 mM Tris/HCl, 100 mM NaCl (pH 7.4) at 4°C. Next, the solution was concentrated to ~200  $\mu$ M using a 10 kDa ultrafiltration device (Amicon; Millipore, Burlington, MA), followed by buffer exchange to water performed by 4-5 concentration-dilution cycles using the same device. Samples were stored at -80°C. In purification of the cysteine-engineered variant MSP1E3D1\_D73C, 5 mM  $\beta$ -mercaptoethanol was added to all the solvents used in the purification process. The molecular weight of the purified MSP1E3D1 scaffold protein variant was determined by mass spectroscopy to be 32,601 Da in agreement with the calculated molecular weight. The hydrodynamic diameter of a typical ND preparation was 12.9 nm as calculated by the retention time on a calibrated size exclusion column and 13.1  $\pm$  2.5 nm as determined by dynamic light scattering measurements on a Malvern Zetasizer Nano instrument (Malvern, UK). Quantum yield (QY) of fluorescent NDs was measured using a commercial quantum yield spectrometer (Quantaaurus-QY C11347; Hamamatsu, Hamamatsu, Japan).

### ND preparation

ND composition was calculated to give a final ratio of 150:1 lipids/MSP with DMPC as the main lipid constituent. In a typical preparation, stock solutions of lipids stored in chloroform were mixed to yield the specific mole ratio composition. The solvent was evaporated using a vacuum concentrator (Labconco, Kansas City, MO) for 20 min at 60°C. The dried film was thoroughly dissolved in 8  $\mu$ L of 20 mM Tris (pH 7.4), 50 mM sodium cholate, and 100 mM NaCl and incubated for 15 min at 40°C with agitation. To the lipid solution, 5  $\mu$ L of a 200  $\mu$ M MSP in water were added to give a final MSP concentration of 70  $\mu$ M. The sample was incubated for 15 min at 40°C with agitation. The solution was added to 7.5 mg of damp adsorbent beads (Amberlite XAD-2; Sigma-Aldrich) preheated to 40°C and incubated at 40°C with agitation for 1 h. The sample was diluted with 100  $\mu$ L PBS, filtered by a 0.22  $\mu$ m polyethersulfone (PES) syringe filter, and stored at 4°C until further use. Sample purity was verified by size exclusion chromatography on a Superdex S-300 10/300 GL column (Pharmacia, Stockholm, Sweden) and by dynamic light scattering (DLS), for samples without Cy5-PE.

### ND-avidin complex preparation

Avidin was dissolved in PBS adjusted to pH 8.6, to a final concentration of 5 mg/mL. 20  $\mu$ L NDs incorporating biotinylated lipids were added slowly to 180  $\mu$ L avidin solution under stirring, and the solution was stirred for 20 min in the dark. The sample was filtered by a 0.22  $\mu$ m PES syringe filter and centrifuged at 20,000 RCF at 4°C for 15 min, and used immediately.

### ND conjugation to Ab

Site-specific conjugation of NDs to anti-GABA<sub>A</sub> receptor  $\gamma$ 2 IgG (Synaptic Systems) by copper-free click chemistry was achieved in three steps. In the first step, NDs were prepared from scaffold proteins incorporating a single point mutation to cysteine (D73C). Solvent exchange of ND samples to HEPES 20 mM, NaCl 150 mM (pH 7.2) was performed by gel filtration using Zeba spin columns (40 kDa MWCO) followed by filtration using a 0.22  $\mu$ m PES syringe filter. Freshly prepared TCEP stock solution was diluted to a final 10-fold of MSP,

and the solution was stirred for 30 min at room temperature to achieve complete reduction of cysteines. A bifunctional linker, maleimide-polyethyleneglycol(24) -dibenzocyclooctyne (Mal-PEG<sub>24</sub>-DBCO) dissolved in dimethyl sulfoxide (DMSO), was added to a final 50-fold over MSP, and the mixture was allowed to react for 1.5 h at room temperature, in the dark, under stirring. Excess reactants were removed by gel filtration using Zeba columns, and the sample was fractionated on a size exclusion column to remove residual reactants that could interfere with further steps. The elution peak was collected and concentrated using an Amicon ultrafiltration device (50 kDa MWCO) to a final ND concentration of ~30  $\mu$ M. The degree of labeling by the linker was evaluated by the molar extinction coefficient of the labeled product to be ~1.2:1 linker/ND (Fig. S3, A and B). In the next step, an IgG polyclonal anti-GABA<sub>A</sub> antibody was modified to contain an azide on the Fc using a dedicated kit (ClickSite). Finally, ND-DBCO and Ab-azide were mixed to yield a 2:1 Ab/ND solution (20  $\mu$ M MSP) and were incubated over night at 35°C in the dark. Sample composition was evaluated by size exclusion chromatography (Fig. S3 C).

### Image acquisition

A 100 $\times$  oil-immersion objective (UAPON100XOTIRF; Olympus, Tokyo, Japan) and an EMCCD camera (iXon Ultra 897; Andor, Belfast, Northern Ireland, UK), coupled to an inverted microscope (IX83; Olympus) with both epifluorescence and TIRF illumination optics, were used for all imaging experiments. A light-emitting diode light source (SPECTRA X; Lumencor, Beaverton, OR) was used for epifluorescence illumination and a laser (iChrome MLE; Toptica Photonics, Graefelfing, Germany) for TIRF illumination.

### Time-resolved fluorescence measurements

Fluorescence lifetime measurements of labeled NDs constructs were performed in a time-correlated time-tagged recording mode using a static confocal excitation and detection spot in the solution. A 470 nm diode laser (LDH-P-C-470B; PicoQuant, Berlin, Germany), connected to a picosecond laser driver (PDL 828 Sepia II; PicoQuant), was coupled to an inverted confocal microscope (SP8; Leica, Wetzlar, Germany), using a 63 $\times$  water-immersion objective (HC PL APO 63 $\times$ /1.20 W; Leica). The emitted light was spectrally filtered at 520  $\pm$  10 and 700  $\pm$  30 nm for TF and Cy5, respectively, and focused onto photodetectors (HyD; Leica). The laser driver and photodetectors were connected to a dedicated time-correlated single photon counting system (PicoHarp 300; PicoQuant) to obtain lifetime curves. ND samples were diluted to 30 nM in PBS and transferred to chambered coverslips for measurement. Lifetime measurements in the presence of DPA were performed on the same well by dilution  $\times$  200 of a stock solution of DPA to a final concentration of 2  $\mu$ M. Lifetime values were calculated using SymPhoTime 64 analysis software (PicoQuant) by fitting the measured decay curves to a three exponents model, convoluted with the instrument response function. The lifetime values described in the text represent the amplitude-weighted average lifetime.

### Photobleaching experiments

#### Coverslip preparation

Measurements were performed on NDs adsorbed to chambered coverslips ( $\mu$ -slide eight well; ibidi, Graefelfing, Germany). Chambers were cleaned by overnight incubation with a 2% Hellmanex III cleaning solution at room temperature, followed by extensive wash with deionized water (DIW) and sonication for 15 min in water to remove residual detergent. Finally, residual fluorescent contaminants were removed by a glow discharge system (Emtech K100 $\times$ ; Quorum Technologies, Lewes, UK) for a total of 3 min.

### Photobleaching measurements

ND samples were diluted  $\times 10^5$  in PBS to a working concentration of  $\sim 30$  pM, and 200  $\mu\text{L}$  of the diluted solution was added to each well. Photobleaching measurements of all samples were performed on the same day. Samples were incubated for 10 min in the dark at room temperature, and the wells were washed six times with PBS. Imaging was performed in a TIRF configuration, using a 488 nm laser line (iChrome MLE; Toptica Photonics) with a total illumination power of 1 mW after the objective. Fluorescence emission of TF and Cy5 were spectrally filtered using a  $520 \pm 10$  nm and a  $700 \pm 30$  nm bandpass filters (Chroma, Bellows Falls, VT), respectively. Image recording was done with 100 ms exposure time and  $300\times$  electron multiplier gain. To obtain complete emission curves not degraded by the photobleaching that occurs while focusing the image, we took the following steps for each imaged region-of-interest (ROI): 1) imaging system was focused on a region  $\sim 100$   $\mu\text{m}$  away from the selected ROI, 2) the excitation beam shutter was closed, 3) the stage was translated  $\sim 100$   $\mu\text{m}$  to the ROI to be used for acquisition, and finally 4) data acquisition was initiated and excitation beam shutter was opened.

### Data analysis of photobleaching measurements

For photobleaching analysis of labeled NDs, we used the Progressive Idealization and Filtering (PIF) counting program (24), a dedicated software for the analysis of data obtained from imaging fluorescence bleaching of multiply labeled complexes, such as single subunit counting of tagged proteins. For our analysis, we used a 15% intensity threshold for spot detection, a  $2\sigma$  limit for proximity threshold between spots, and a threshold of 2.5 step/noise. Analysis parameters were identical for all data sets.

### HEK293 and primary cortical neuron culture

HEK293 cells were cultured in Dulbecco's modified Eagle's medium containing 10% fetal calf serum, 2 mM glutamine, 100 units/mL penicillin G, and 100  $\mu\text{g}/\text{mL}$  streptomycin and grown in 5%  $\text{CO}_2$  at  $37^\circ\text{C}$  under 90–95% humidity. For electrophysiology experiments, the cells were seeded on glass coverslips (25 mm diameter) that were placed in six-well plates and precoated with poly-D-lysine. Electrophysiology experiments were performed 24–48 h after seeding. Cells were plated at a 1:5 or 1:10 dilution onto poly-D-lysine-coated six-well 3–5 days before an experiment. Experiments were performed with 70% confluent cells. All animal experiments were approved by the local ethics committee for animal research (ethical approval number 63-09-2018). Primary cortical neurons were cultured from P1 and P2 newborn Sprague-Dawley rats. The tissue was digested by 100 units of papain (Sigma-Aldrich) in  $\text{Ca}^{2+}/\text{Mg}^{2+}$ -free Hank's balanced salt solution (Biological Industries, Beit HaEmek, Israel) in  $37^\circ\text{C}$  incubator. The tissue was then mechanically dissociated, and the cells were plated on 50  $\mu\text{g}/\text{mL}$  of poly-D-lysine-coated cover glasses in neurobasal medium (Biological Industries) supplemented with 2% B-27 (Invitrogen, Carlsbad, CA), GlutaMAX-1 2 mM (Invitrogen), the antibiotics penicillin (100 unit/mL)/streptomycin (100  $\mu\text{g}/\text{mL}$ ) (Beit HaEmek 030311B), glucose, and 5% normal horse serum (Biological Industries). On the following day and twice a week thereafter, medium was exchanged with growth medium; once a week, the medium was applied with Ara-C to prevent glial proliferation. Cell were incubated at  $37^\circ\text{C}$  in humidified air containing 5%  $\text{CO}_2$ .

### Colocalization, staining, and transfection

Cortical neuron cultures were prepared and grown on glass coverslips (25 mm diameter), precoated with poly-D-lysine, and placed in six-well plates. Cells were transfected after 9 days in vitro with pmCherryC2-Gephyrin P1, a gift from Shiva Tyagarajan (Addgene plasmid #68820; <http://www.addgene.org/68820/>; RRID: Addgene\_68820).

Transfection was performed using Lipofectamine 3000 (Invitrogen) according to the manufacturer's instructions (12  $\mu\text{L}$  of Lipofectamine 3000 and 2.8  $\mu\text{g}$  per well). Expression was confirmed after 24 h by fluorescence microscopy. The  $\text{ND}_{\text{TF,Cy5}}\text{-Ab}$  conjugate was diluted in fresh cell culture medium and applied directly to the well containing the live cells 24 h after transfection. The  $\text{ND}_{\text{TF,Cy5}}\text{-Ab}$  conjugate was incubated for 10 min at  $37^\circ\text{C}$  in a 5%  $\text{CO}_2$  incubator. Subsequently, the cells were washed twice with neuronal external solution.

### Patch-clamp experiments

#### Electrophysiological recording

Whole-cell voltage-clamp recordings in HEK cells were performed using a computer-controlled amplifier (EPC 10 USB; HEKA Elektronik, Reutlingen, Germany). Recorded signals were filtered at 10 kHz using a Bessel filter and digitized at 10–100 kHz, depending on the time-scale of the voltage waveform.

The external solution for HEK cells contained 140 mM NaCl, 2.8 mM KCl, 2 mM  $\text{CaCl}_2$ , 1 mM  $\text{MgCl}_2$ , 10 mM HEPES, and 10 mM glucose, adjusted with NaOH to pH 7.4 (310 mOsm). The pipette solution contained 125 mM potassium gluconate, 0.6 mM  $\text{MgCl}_2$ , 0.1 mM  $\text{CaCl}_2$ , 1 mM EGTA, 10 mM HEPES, 4 mM Mg-ATP, 0.4 mM  $\text{Na}_2\text{GTP}$ , adjusted with KOH to pH 7.4 (295 mOsm). The electrode resistance was 5–10  $\text{M}\Omega$  when filled with the pipette solution.

For neural cells, all imaging and electrophysiology experiments were conducted with a neuronal external solution containing 116.9 mM NaCl, 2.7 mM KCl, 1.8 mM  $\text{CaCl}_2$ , 0.5 mM  $\text{MgCl}_2$ , 20 mM HEPES, 5.5 mM glucose, 0.36 mM  $\text{NaH}_2\text{PO}_4$ , 200 mM ascorbic acid, and penicillin (100 unit/mL)/streptomycin (100  $\mu\text{g}/\text{mL}$ ) at pH 7.3 and adjusted to 320 mOsm with sucrose. The pipette solution contained 110 mM potassium gluconate, 10 mM KCl, 10 mM glucose, 8 mM sodium creatine-phosphate, 5 mM EGTA, 10 mM HEPES, 4 mM Mg-ATP, 0.4 mM Na-GTP (pH 7.3), adjusted to 290 mOsm with sucrose.

#### Optical recording

Imaging was performed using a light-emitting diode light source passing through a 470/24 nm bandpass filter and an EMCCD camera (iXon Ultra 897; Andor), coupled to a motorized inverted microscope (IX83; Olympus). All imaging was performed using a  $100\times$  oil-immersion objective (UAPON100XOTIRF; Olympus). Fluorescence emission was filtered with a bandpass filter centered at 590 nm for mCherry (ET590/33m; Chroma), and centered at 700 nm for Cy5 (ET700/75m; Chroma). A data acquisition (DAQ) device (USB-6211; National Instruments, Austin, TX), controlled by home-written software (LabVIEW; National Instruments), was used for synchronizing the camera and the patch-clamp amplifier.

#### Data analysis

Analysis of fluorescence imaging of clamped cells was performed in MATLAB (The MathWorks, Natick, MA). For sparse staining, a two-dimensional particle tracking algorithm was used to correct for small translations. Fluorescence intensity for each frame was calculated by averaging the 10 brightest pixels of each spot for sparse staining and averaging the fluorescence from the whole cell for ensemble measurements. For the latter, background subtraction of each frame was performed by subtracting the mean value of the 10% darkest pixels. Fluorescence trajectories were corrected for photobleaching by either a shortpass filter or subtraction of the fluorescence trajectory by a two-term exponential function fitted to the baseline voltage levels. The average optical voltage response curve for each intensity trace was calculated by averaging the emission intensity corresponding to every voltage level throughout the trajectory. To achieve a stabilized value of the response, the averaging was performed on the frames containing the last 100 ms of each voltage step.

## Data availability

Raw data of all fluorescent imaging from all electrophysiological recordings and fluorescence lifetime measurements for this work can be found here: <https://zenodo.org>, <https://doi.org/10.5281/zenodo.4704309>. Home-written code (MATLAB) for the extraction and analysis of recorded electrophysiological optical trajectories is available upon request.

## RESULTS

To investigate whether donor labeled NDs can perform as membrane potential sensors via FRET to DPA, we labeled NDs with TF, a BODIPY derivative labeled at the headgroup of a PE lipid. This bright and stable lipid-labeled fluorophore has a high extinction coefficient of  $96,904 \text{ mol}^{-1} \text{ cm}^{-1}$  in MeOH, a QY of 0.9, and it incorporates spontaneously into the ND bilayer during the self-assembly process.

Initial experiments showed that the emission from labeled NDs adsorbed either to the plasma membrane of HEK293 cells or to a coverslip glass surface was completely quenched in the presence of  $2 \mu\text{M}$  DPA in solution. This quenching is attributed to very high energy transfer efficiencies from TF to DPA molecules. The effect was reversible to some extent after several wash cycles and removal of DPA from the solution, thereby indicating that quenching occurs to either DPA molecules dissolved in solution, DPA molecules dissolved in the ND bilayer, or both.

To solve this detrimental effect, we employed two strategies aimed at 1) limiting the accessibility of water-soluble DPA from the vicinity of solvent-exposed dyes and 2) reducing energy transfer efficiency to DPA (Fig. 1).

### ND bilayer surface capping by biotin-avidin interactions

To limit the accessibility of DPA molecules to the vicinity of ND-embedded dyes, biotinylated lipids were added to the ND composition. Avidin was conjugated to the solvent-exposed biotin groups in the assembled ND to form a steric barrier to DPA molecules. To ensure tight binding between avidin and the ND surface, we used biotinylated lipids with a short spacer that permits only the solvent-exposed biotin group to penetrate into the avidin-binding site, leaving no space for avidin translational motion. Furthermore, reaction parameters (biotinylated lipid concentrations, incubation time, avidin concentration, solution pH) were optimized to enhance the probability for multivalent binding of avidin to the ND surface (25,26), thus increasing the contact area between avidin and the ND bilayer surface. This was achieved at a 40% mol ratio of biotinylated lipids/total ND lipids in the preparation mixture.

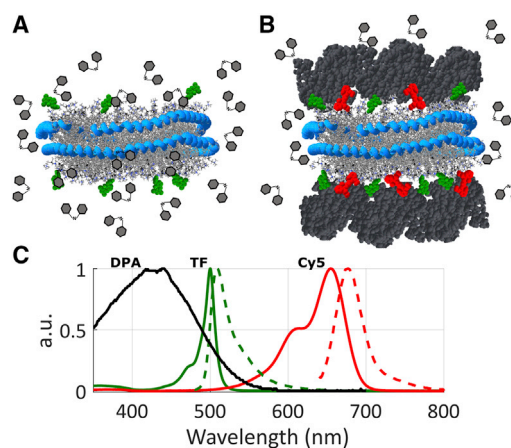


FIGURE 1 Scheme of functionalized NDs. (A) NDs labeled by TF (green) in the presence of DPA (gray hexagons). DPA is in both the solvent and the ND bilayer. (B) NDs labeled by TF and Cy5-PE (red). The ND bilayer surface is capped by avidin (dark gray), which restricts the distance between DPA and TF. (C) The absorbance (solid) and emission (dashed) spectra of  $\text{ND}_{\text{TF}}$  (green) and  $\text{ND}_{\text{Cy5}}$  (red) and absorbance spectrum of  $2 \mu\text{M}$  DPA (black). Absorbance and emission spectra were measured for  $\text{ND}_{\text{TF}}$  at  $\sim 10:1$  TF/ND ratio and  $\text{ND}_{\text{Cy5}}$  at  $\sim 4.5:1$  Cy5/ND. All spectra were recorded in PBS buffer at  $20^\circ\text{C}$ . The overlap between the emission of  $\text{ND}_{\text{TF}}$  and the absorbance of  $\text{ND}_{\text{Cy5}}$  allows efficient energy transfer.

Avidin binding was confirmed by an observed hydrodynamic diameter increase from  $13.1 \pm 2.5$  to  $27.2 \pm 4.6$  nm, determined by DLS measurements. Considering that the hydrodynamic diameter of free avidin is  $7.4 \pm 1.3$  nm, the increase in diameter represents avidin binding to both facets. Incubation of biotin-free NDs with avidin under the same conditions resulted in large aggregates of  $>100$  nm in diameter, further supporting specific biotin-avidin association (Fig. S1). We note that nominal biotin concentrations lower than 40% were found to bind to avidin, manifested by a similar increase of hydrodynamic diameter of ND-avidin conjugates. However, these conjugates were not resistant to quenching by DPA, indicating nonmultivalent avidin binding.

### Incorporation of a competing fluorescent acceptor into the ND bilayer

To provide an efficient competing route to energy transfer from TF to DPA, we incorporated a second acceptor into the ND bilayer. We hypothesized that at high dye densities of TF and a second fluorescent acceptor, both confined to the ND bilayer, the average distance between the dyes would be short enough to produce high FRET efficiencies to effectively compete with excessive energy transfer to the soluble fraction of DPA molecules (which do not participate in membrane potential sensing). To that end, a Cy5 derivative conjugated to the headgroup of a PE lipid (Cy5-PE)

was selected as a second acceptor to the TF donor. This dye incorporates into the ND bilayer during self-assembly; it has a high extinction coefficient of  $220,000 \text{ mol}^{-1} \text{ cm}^{-1}$  in DMSO and a QY of  $0.51 \pm 0.05$  when embedded into NDs. It is spectrally resolved from TF and has a Förster radius of  $35.4 \text{ \AA}$  as the acceptor to TF.

### Optimization of labeled ND brightness

To determine the optimal number of TF dyes that would maximize the brightness of labeled NDs, the QY dependence on the number of TF and Cy5-PE was determined. This is necessary because the confined volume of the ND bilayer only allows for a finite number of dyes to be incorporated before reduction of brightness due to self-quenching and photon reabsorption begins to degrade the photophysical properties of the dyes. By preparing NDs with an increasing number of labeled lipids, we observed that the brightness continued to increase upon the addition of labeled lipids until it reached ratios of 6:1 TF/ND for  $\text{ND}_{\text{TF}}$  and 4:1 Cy5-PE/ND for  $\text{ND}_{\text{Cy5}}$ . A detailed description of this characterization is given in Fig. S2. Above six TF molecules per ND and above four Cy5-PE molecules per ND, self-quenching greatly decreased the contribution of additional incorporated TF or Cy5 molecules to the construct's brightness.

We note that the brightness of NDs labeled with TF at a 6:1 TF/ND ratio is very high compared to commercially available labels with a similar emission range used in biological applications. For example, the brightness of commercial streptavidin-conjugated quantum dots (QD525) is only  $\sim 35\%$  of  $\text{ND}_{\text{TF}}$  incorporating six TF dyes (27) and that of antibodies conjugated to Alexa 488 dyes at a working degree of labeling of three is only  $\sim 50\%$  (28).

### Evaluation of labeled ND quenching by DPA

In the presence of  $2 \mu\text{M}$  of DPA, which is a common working DPA concentration for FRET-based membrane potential measurements, the fluorescence from  $\text{ND}_{\text{TF}}$  with a ratio of 6:1 TF/ND was completely quenched. To test and compare the efficiency of the two approaches in reducing TF quenching by DPA, four labeled ND samples were prepared using 14 TF dyes per ND, which was enough to maintain sufficient fluorescence in the presence of DPA: 1) ND labeled with donor only at a molar ratio of 14:1 TF/ND ( $\text{ND}_{\text{TF}}$ ) and 2) ND labeled with both donor and acceptor at a molar ratio of 14:6:1 TF/Cy5/ND ( $\text{ND}_{\text{TF,Cy5}}$ ). Both samples contained biotinylated lipids at a 40% molar ratio in the preparation mixture. Samples (1) and (2) were diluted  $\times 10$  to a  $5 \text{ mg/mL}$  avidin solution in PBS (pH 8.6) and incubated for 30 min at room temperature while stirring to produce samples of 3)  $\text{ND}_{\text{TF}}$ -avidin and 4)  $\text{ND}_{\text{TF,Cy5}}$ -avidin. All samples were filtered using a  $0.22 \mu\text{m}$  syringe filter immediately before measurement. For photobleaching measurements of NDs adsorbed to a coverslip glass, the same samples were prepared with the addition of 3% DC-cholesterol to add cationic charge to promote ND interaction with glass.

DPA quenching efficiency was evaluated by fluorescence lifetime measurements for samples in solution (Fig. 2) and by photobleaching kinetics imaging of labeled NDs adsorbed on a glass coverslip. From the photobleaching trajectories, we determined the average emission intensity for a single ND and survival time, defined as the total emission time for each ND under constant illumination (as further described in Materials and methods). The quantification of these parameters allowed us to evaluate the effect of DPA on the photophysical properties of different ND compositions and is summarized in Table 1. The fluorescence lifetime for TF in  $\text{ND}_{\text{TF}}$ , which was measured to be

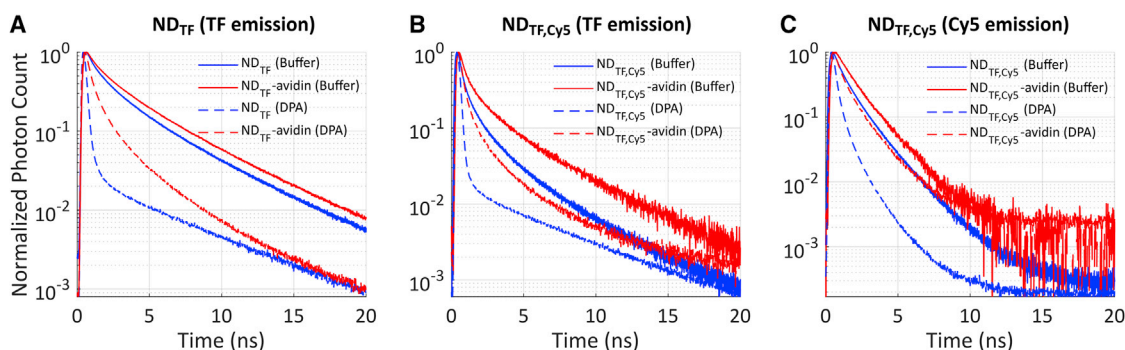


FIGURE 2 Fluorescence lifetime histograms of labeled NDs. Labeled ND samples were diluted into PBS to a final  $30 \text{ nM}$  in chambered coverslips and the fluorescence lifetime was recorded using a  $485 \text{ nm}$  laser excitation with a  $520 \pm 10 \text{ nm}$  emission filter for TF and a  $700 \pm 30 \text{ nm}$  for Cy5-PE. The normalized fluorescence lifetime decay curves are shown for NDs labeled with (A) TF only or (B and C) both TF and Cy5-PE, with (B) and (C) showing the fluorescence lifetime emission of TF and Cy5, respectively. Samples were measured in buffer (continuous lines) and in buffer +  $2 \mu\text{M}$  DPA (dashed lines) for avidin-free (blue lines) and avidin-conjugated (red lines) constructs.

**TABLE 1 Photophysical properties of labeled NDs in buffer and in buffer with 2  $\mu$ M DPA**

	Sample ID	ND <sub>TF</sub>	ND <sub>TF,Cy5</sub>		ND <sub>TF-avidin</sub>	ND <sub>TF,Cy5-avidin</sub>	
	emission filter <sup>a</sup>	TF	TF	Cy5	TF	TF	Cy5
Buffer	fluorescence lifetime (ns) <sup>b</sup>	2.23	0.8	1.04	2.82	1.48	1.39
	survival time (s) <sup>c</sup>	–	4.35	1.1	–	3.46	1.2
	intensity (a.u.) <sup>d</sup>	~0	0.31	0.99	~0	0.43	1.00
Buffer + DPA	fluorescence lifetime (ns) <sup>b</sup>	0.36	0.47	0.38	0.96	0.65	0.89
	survival time (s) <sup>c</sup>	–	6.77	4.4	–	3.9	3.2
	intensity (a.u.) <sup>d</sup>	~0	0.15	0.39	~0	0.12	0.28
	#NDs with DPA/#NDs without DPA <sup>e</sup>	~0	0.05	0.08	~0	0.31	1

<sup>a</sup>Fluorescence emission was detected at a  $520 \pm 10$  nm and a  $700 \pm 30$  nm spectral range for TF and Cy5 emission, respectively.

<sup>b</sup>Fluorescence lifetime was collected for samples freely diffusing in solution using a 470 nm pulsed excitation.

<sup>c</sup>Survival time was defined as the characteristic total emission time of a single ND adsorbed to a glass surface.

<sup>d</sup>Mean ND intensity was defined as the average intensity for a population of NDs adsorbed to glass at the onset of illumination, with values normalized to the highest intensity measured. Adsorbed NDs were all excited at 488 nm using a constant illumination intensity.

<sup>e</sup>The proportion of detectable NDs per ROI in the presence of DPA relative to NDs detected in buffer. Evaluation was performed on the same glass surface.

2.23 ns in buffer without DPA, reduced to 0.8 ns with the addition of Cy5 in ND<sub>TF,Cy5</sub> because of an expected high FRET efficiency between TF and Cy5-PE. However, the contribution of Cy5-PE to the photostability of TF in the presence of DPA is small, as shown in Table 1. This was also observed for glass-adsorbed ND<sub>TF,Cy5</sub>, for which only ~8% of the NDs detected in buffer were detectable in the presence of 2  $\mu$ M DPA, and with a ~50 and ~60% decrease in the mean intensity for TF and Cy5-PE, respectively.

For the avidin-conjugated samples, the fluorescence lifetime of TF for ND<sub>TF-avidin</sub> in buffer, increased from 2.23 to 2.82 ns, reflecting the change in the chromophore molecular environment. The lifetime for TF and Cy5-PE in ND<sub>TF,Cy5-avidin</sub> was longer compared to the avidin-free construct, but the photobleaching trajectories for both samples in buffer were similar. In the presence of DPA, lifetime decay curves of both TF and Cy5-PE in ND<sub>TF,Cy5-avidin</sub> regained similarity to the decay curves of ND<sub>TF,Cy5</sub> in buffer. This was also manifested in the properties of glass-adsorbed ND<sub>TF,Cy5-avidin</sub>. The amount of detectable TF and Cy5-PE in DPA compared to buffer for glass-adsorbed ND<sub>TF,Cy5-avidin</sub> was 30 and 100%, respectively. Interestingly, the survival time of Cy5 was threefold higher compared to that measured in buffer. Moreover, although the recovery and survival time were higher, the mean intensity per ND was 20% for TF and 30% for Cy5 compared to the intensity recorded in buffer. The above leads to conclude a synergistic mechanism for sustainable dye emission in the presence of DPA, involving both surface capping by avidin and incorporation of an additional energy transfer channel for TF.

### Membrane potential sensing in HEK293 cells

The performance of ND<sub>TF,Cy5-avidin</sub> constructs as membrane potential sensors was first evaluated on the ensemble and single-particle level using HEK293

cells as a model system. Cells were stained with 5 nM ND<sub>TF,Cy5-avidin</sub>, showing a high degree of staining (Fig. 3 B). The optical response of HEK293 labeled with ND<sub>TF,Cy5-avidin</sub> in a 2  $\mu$ M DPA solution was measured by exciting TF at 470 nm and detecting the emission of Cy5 while voltage clamping the cells to different values of membrane potential, stepping between –80 and 80 mV with 20 mV steps of 200 ms in duration, as shown in Fig. 3. The average optical response, defined as the relative change in fluorescent emission  $\Delta F/F$  from a total of five cells, was measured to be  $33 \pm 6.4\%$  per 120 mV (Fig. 3 E). We note that all imaging of voltage-dependent fluorescence emission was performed in the spectral regime of the acceptor fluorophore Cy5 because it had a considerably better signal/noise ratio than the donor fluorophore TF.

The response kinetics of ND<sub>TF,Cy5-avidin</sub> was not instantaneous with the change in membrane potential and was limited to the detection of transient changes at the 10 ms scale and above, as further described in Fig. S4. The response fall time, defined as the duration needed for the fluorescent emission to decay from 90 to 10% from its maximal intensity value once a 100 ms pulsed polarization ends, was measured to be 220 ms. We note that similar kinetics was observed when cells were directly stained with TF-PE-labeled lipids. Because the DiO-DPA FRET pair respond to changes in membrane potential at submillisecond time-scales (23), it is likely that the fluorescent donor group of ND<sub>TF,Cy5</sub> is also translocated by the change in membrane potential (29). Another possibility for the slow response could be a slow mechanical translocation of the ND itself between membrane-tight and membrane-loose bound states (to be investigated in a future work).

### Membrane potential sensing in neurons

Primary cortical neurons were stained with ND<sub>TF,Cy5-avidin</sub> to achieve membrane labeling on the single-

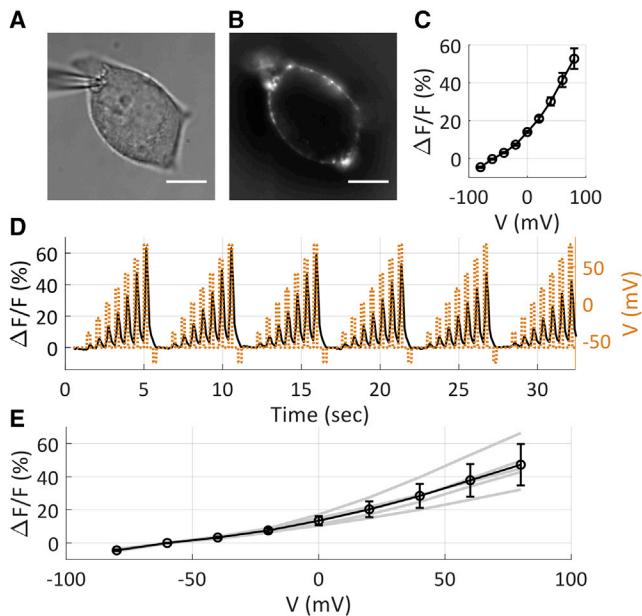


**FIGURE 3** Fluorescence response of  $\text{ND}_{\text{TF,Cy5}}\text{-DPA}$  to changes of membrane potential in HEK293 cells. Cells were stained with  $\text{ND}_{\text{TF,Cy5}}$  and voltage clamped in the presence of  $2\ \mu\text{M}$  DPA. (A) Differential interference contrast (DIC) image and (B) Cy5 fluorescence emission of a patch-clamped HEK293 cell. Scale bars,  $10\ \mu\text{m}$ . (C) The average change and (D) signal trajectory of Cy5 fluorescence emission as a function of membrane potential, relative to the emission at  $-60\ \text{mV}$ . Average was calculated over six consecutive voltage steps. The voltage waveform consisted of varying voltage levels with  $20\ \text{mV}$  steps for  $200\ \text{ms}$  at each voltage level and a  $400\ \text{ms}$  resting period of  $-60\ \text{mV}$ . Optical recording was done at  $10\ \text{Hz}$  frame rate. Error bars represent the SD of the fluorescence change between consecutive voltage potential sweeps. (E) Fluorescence response curves of five individual cells (gray), calculated by averaging the response from six consecutive voltage steps, and the averaged response (black). Error bars represent the SD of the averaged response values.

particle level. Staining conditions were similar to those applied for ensemble labeling of HEK293 cells; however, because of lower membrane adsorption efficiency to neurons, the resulting ND labeling was sparse. Neurons were voltage clamped in a solution containing  $2\ \mu\text{M}$  DPA, and the optical response of single  $\text{ND}_{\text{TF,Cy5}}\text{-avidin}$  to changes in membrane potential was recorded. Membrane potential was alternated between  $-60, 0,$  and  $60\ \text{mV}$ . Imaging was performed by exciting TF at  $470\ \text{nm}$  and detecting the emission of Cy5. A representative example of the optical response of localized  $\text{ND}_{\text{TF,Cy5}}\text{-avidin}$  staining on neuronal soma is shown in Fig. 4. The average response  $\Delta F/F$  of  $24\ \text{ND}_{\text{TF,Cy5}}$  particles, measured from a total of five cells, was  $23.1 \pm 16\%$  per  $120\ \text{mV}$ . We note that all the single fluorescent spots were responsive to changes in membrane potential, showing a change of fluorescent emission of at least  $2\%$  per  $120\ \text{mV}$ . These results clearly demonstrate the ability of  $\text{ND}_{\text{TF,Cy5}}\text{-avidin}$  to probe neuronal membrane voltage changes from single local-

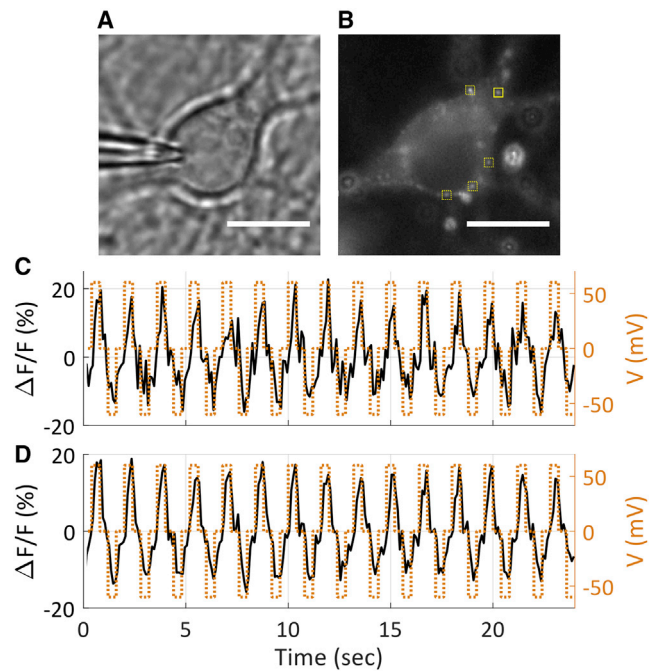


**FIGURE 4** Fluorescence response of  $\text{ND}_{\text{TF,Cy5}}\text{-DPA}$  to changes of membrane potential in primary cortical neuron cells at low  $\text{ND}_{\text{TF,Cy5}}$  loading. Cells were stained with  $\text{ND}_{\text{TF,Cy5}}\text{-avidin}$  and voltage clamped in the presence of  $2\ \mu\text{M}$  DPA. (A) DIC image and (B) Cy5 fluorescence emission of a patch-clamped primary cortical neuron. Scale bars,  $10\ \mu\text{m}$ . The cells were clamped to a square voltage waveform consisting of  $0, 60, 0,$  and  $-60\ \text{mV}$  voltage levels, each  $400\ \text{ms}$  in duration. (C) shows the change in Cy5 fluorescence emission as a function of membrane potential from  $\text{ND}_{\text{TF,Cy5}}$  in the region inside the solid yellow square. Averaged response was  $26.4 \pm 5.2\%$  per  $120\ \text{mV}$ . (D) The averaged fluorescence of five  $\text{ND}_{\text{TF,Cy5}}$  particles indicated by yellow squares, showing an averaged response of  $27.1 \pm 3.3\%$  per  $120\ \text{mV}$ .

ized spots. We note that the response for different  $\text{ND}_{\text{TF,Cy5}}$  was found to be significantly heterogeneous, as demonstrated in Fig. S5, in which we show the averaged optical response to changes in membrane potential at each pixel of the imaged area. This variability in response may occur from the heterogeneity of NDs such as the number of dyes or avidin-binding biotin molecules incorporated in each ND bilayer; from the variability in the mode of interaction between the NDs, cell membrane, and the surrounding DPA molecules; and, to a lesser extent, because of local differences in membrane potential occurring in whole-cell patch clamping of neurons.

### Site-directed membrane potential sensing in neurons

To demonstrate membrane potential sensing from specific neuron sites, we selected to target  $\text{ND}_{\text{TF,Cy5}}$  to  $\text{GABA}_A$  receptors ( $\text{GABA}_A\text{Rs}$ ). Depending on their subunit composition,  $\text{GABA}_A\text{Rs}$  can be found on the

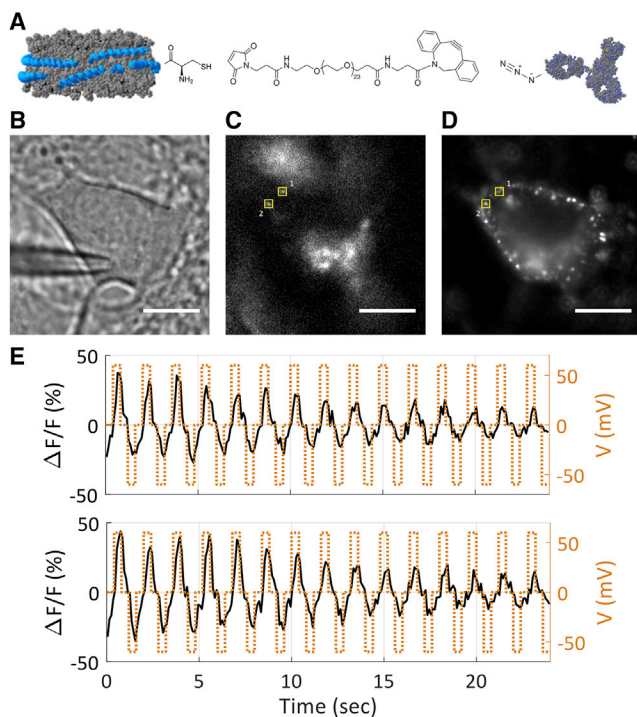


FIGURE 5 Single-particle membrane potential optical recordings from ND<sub>TF,Cy5</sub>-Ab-avidin complex targeting GABA<sub>A</sub>R and DPA. Cultured cortical neurons were transfected with mCherry-gephyrin and stained with ND<sub>TF,Cy5</sub> conjugated to Ab-GABA and avidin. Cells were voltage clamped in the presence of 2  $\mu$ M DPA. (A) ND-Ab conjugation scheme, using Mal-PEG(24)-DBCO as a bifunctional linker. (B) DIC image of a patched cortical neuron, expressing mCherry-gephyrin and labeled with ND<sub>TF,Cy5</sub>-Ab-avidin. (C) and (D) show the emission of mCherry and Cy5, respectively. Scale bars, 10  $\mu$ m. (E) shows the changes in Cy5 fluorescence emission as a function of membrane potential from the two ND<sub>TF,Cy5</sub> (1, top; 2, bottom) in the regions inside the solid yellow squares. The average change in emission fluorescence was measured to be 1)  $35.7 \pm 14.4\%$  and 2)  $45.7 \pm 20.1\%$  per 120 mV.

postsynaptic side of the synapse and also on soma and dendrites (30,31). We used anti-GABA<sub>A</sub>R  $\gamma$ 2 (Ab-G) as the recognition element for conjugation to ND<sub>TF,Cy5</sub>. Ab-G targets the  $\gamma$ 2 subunit, which is present in GABAergic synaptic junctions in the hippocampus, cerebellum, and most cortical synapses (32,33). To that end, ND<sub>TF,Cy5</sub> were cross-linked to Ab-G via a hydrophilic linker to reduce potential undesired interactions between Ab-G and ND<sub>TF,Cy5</sub> (ND-Ab) (Fig. 5 A). Cell labeling was performed by incubation of ND-Ab with the neuron culture to allow for Ab-G-driven membrane association, followed by a wash step and a short incubation with avidin to achieve ND bilayer capping by avidin and a strong membrane adsorption via the cationic charge of avidin. Fig. S6 shows a comparison between the staining of cortical neurons with nontargeting ND<sub>TF,Cy5</sub>-avidin and targeting ND<sub>TF,Cy5</sub>-Ab-avidin, with the Ab-conjugated construct showing a considerable higher degree of staining.

To test for proper targeting, we transfected the cultured neurons with gephyrin fused to mCherry. Gephyrin is a cytoplasmic protein that accumulates at the postsynaptic complex of GABAergic and glycinergic synapses, where it forms submembranous lattices associated with postsynaptic clusters of GABA<sub>A</sub>Rs and glycine receptors, respectively (34). Fig. S7 shows colocalization between ND<sub>TF,Cy5</sub>-Ab-avidin and mCherry-gephyrin for five neurons, demonstrating specific binding of the ND-Ab construct to gephyrin. Next, we tested the Ab-conjugated ND construct as an optical indicator for membrane potential. Figs. 5 and S8 show colocalization and fluorescence response to changes in membrane potential of transfected neurons stained with ND-Ab-avidin. Colocalizations between mCherry-gephyrin and ND-Ab-avidin (indicated by yellow squares) confirm successful targeting of GABA<sub>A</sub>Rs. Negligible staining was observed when performed with similar concentrations of ND without the conjugated antibody, supporting mainly specific binding of the conjugated ND. We note that ND-Ab is expected to also bind to GABA<sub>A</sub>R  $\gamma$ 2, which is colocalized with nonlabeled endogenous gephyrin.

Optical voltage response of ND<sub>TF,Cy5</sub>-Ab-avidin that appeared colocalized with mCherry-gephyrin, implying successful targeting, was measured by voltage clamping the neurons to a waveform alternating between  $-60$ ,  $0$ , and  $60$  mV. Optical response of Cy5 fluorescence to changes in membrane potential for the two targeted ND<sub>TF,Cy5</sub> shown in Fig. 5 were 1)  $35.7 \pm 14.4\%$  and 2)  $45.7 \pm 20.1\%$  per 120 mV. As can be seen from Fig. 5 E, the average error, defined as the standard deviation (SD) over the whole measurement trajectory, is mainly attributed to the considerable photobleaching of the labeled NDs during optical recording. In addition, the average response to changes in membrane potential was observed to be significantly heterogeneous. This heterogeneity in photostability and voltage response could be the result of the heterogeneity of the NDs themselves, in terms of fluorophore labeling and avidin binding, and their interaction with the surrounding DPA quencher.

## DISCUSSION

We have demonstrated rational design and construction of multifunctional NDs for membrane potential sensing from specific sites in neurons. This was achieved by the unique chemical environment and precise self-assembly of NDs, which affords modularity and custom modifications of ND composition. The capability of packing a large number of lipophilic dyes resulted in high brightness. We suggest that the performance of fluorescent NDs can be further

improved by the optimization of lipid composition and by the inclusion of other photostabilizers, such as triplet-state scavengers, to create self-healing nanoparticles and that such improvements could extend the general applicability of labeled NDs to other biological applications.

Compared with voltage-sensing quantum dots and nanorods (NRs), labeled NDs provide an ideal solution for *in vivo* applications because they are nontoxic and biodegradable and contain functional groups for bioconjugation either as amino acid headgroups of the membrane scaffold protein or as functionalized lipid headgroups incorporated into the ND. Moreover, labeled NDs may provide an environmentally friendly and competitive solution to the toxic fluorescent nanoparticles currently employed in other biomedical imaging applications (beyond voltage sensing).

Here, we applied a FRET-based voltage-sensing scheme based on a stationary, membrane-adsorbed ND (donor) and DPA (acceptor), a hydrophobic ion that translocates across the membrane in response to changes in membrane potential. The initial motivation to apply this sensing scheme was that donor dyes can be nonselectively incorporated into the ND bilayer, i.e., voltage sensing does not depend on a facet-selective labeling of the ND bilayer. A major obstacle for utilization of this sensing scheme was the high sensitivity of TF-labeled NDs to quenching by DPA molecules in the buffer solution. We minimized this sensitivity by introducing a competing acceptor fluorophore to the ND bilayer and further improved it by capping the ND surface with avidin. These modifications restored the fluorescence emission from NDs in the presence of DPA in the solution. These strategies convey two additional advantages. First, shifting the voltage-dependent emission to longer wavelengths results in considerably better signal/noise ratio because of reduced background fluorescence. Second, the positively charged avidin promotes adsorption to cell membranes, resulting in better staining of the cell membrane.

We note that the addition of a competing de-excitation transition route to TF through FRET to Cy5 may decrease the overall sensitivity of the TF-DPA pair to changes in membrane potential. The average emission intensity of TF  $F_{TF}$  through direct TF or indirect Cy5 emission channels is proportional to  $k/k_T$ , where  $k$  is the radiative transition rate of TF or the FRET rate to Cy5 and  $k_T$  is the sum of all radiative and nonradiative de-excitation transition rates of TF. Assuming the only voltage-dependent component of  $k_T$  is the nonradiative transfer of energy to DPA  $k_{DPA}(V)$ , the relative change in emission due to small changes in membrane potential is  $\Delta F/F = -\Delta k_{DPA}(V)/k_T$ . Therefore, an additional de-excitation route to TF inevitably reduces its sensitivity

to changes in membrane potential. However, because the autofluorescent background of live cells is considerably weaker in Cy5's red spectral range compared to TF's green spectral range, imaging NDs that contain a TF and Cy5 FRET pair results in a better optical signal/noise ratio for the detection of changes in membrane potential, especially at the single-particle level.

Neuron and HEK293 cell membrane labeling with NDs was achieved by staining with NDs preformed with avidin bound to the ND bilayer. Because the positively charged avidin drives adsorption to the cell membrane, it is not likely that ND<sub>TF,Cy5</sub>-avidin binds parallel to the membrane because the distance gap by avidin should substantially reduce TF energy transfer efficiencies to DPA. It is therefore plausible that in this case, NDs bind perpendicular to the membrane.

A limiting factor for using the ND<sub>TF,Cy5</sub> construct reported here for action potential sensing is its low temporal response. Using ND<sub>TF,Cy5</sub>, we were able to measure changes in membrane potential occurring at down to 10 ms, whereas action potentials are on the submillisecond timescale. One possible explanation is the observation that the temporal response measured for HEK293 labeled by TF is also slow, and therefore, it is only a matter of dye properties. To test this hypothesis, we performed voltage imaging of cells labeled by DiO and cells labeled by ND<sub>DiO</sub> and found that although DiO showed a fast temporal response, it was not the case for ND<sub>DiO</sub>, which points to ND-related hindered temporal response. A similar slow temporal response was also observed, with fluorescent polystyrene beads acting as membrane potential sensors on the nanoparticle level (35). The observation of slow temporal response for two different types of nanoparticles points toward a similar underlying mechanism related to membrane adsorption. The reason for this slow temporal response of nanoparticles and for the slow response of the TF-DPA system is the subject of future studies.

Furthermore, incorporation of VSDs into NDs (that do not rely on FRET) would be the preferred system of choice, as it combines the credibility and proven performance of VSDs together with the feasibility to perform voltage imaging at the nanoscale or single-particle level.

Because the optical response of most VSDs to electric fields is orientation dependent, asymmetric leaflet labeling is necessary for optimal voltage sensitivity. Future developments will include facet-selective inclusion of VSDs into nanodiscs to provide a single component sensor.

The confined space of NDs allows for high-density packing of lipids and functionalized lipids. This property can be advantageous in designing a chemical composition that can enhance different aspects of

the construct, such as photostability, which will allow for long-term nanoscale imaging. For example, similar to water-soluble self-healing dyes (36), NDs can contain labeled lipids coencapsulated with functionalized lipids with a triplet-state scavenger such as nitrophenyl-acetic acid, nitrophenyl-propanoic acid, or nitrophenylalanine as the photostabilizer. Optimizing the dye/stabilizer ratio may yield a highly stable fluorescent complex. Another potential approach would be incorporation of the hydrophobic  $\alpha$ -tocopherol, a natural antioxidant, into the ND bilayer. In the presence of ascorbic acid in solution as the replenisher, this system may prove an efficient photostable enhancing system (37).

In summary, we demonstrated a novel, to our knowledge, platform for engineered fluorescent nanoparticles. Using NDs as an encapsulating agent, we established a nanoscale optical indicator for membrane potential. For that purpose, we utilized NDs that contained several functional components, with two fluorescent dyes that act as an FRET pair, a biotinylated functional group, and an antibody for biological targeting. Together with DPA as a voltage-dependent acceptor, the coupling between NDs and DPA provided a nanoscale voltage-sensitive three-component FRET system. Beyond optical electrophysiology, the ND platform has the potential to become the foundation for a multitude of different functional molecules, offering an extremely versatile framework of nanoscale particles for imaging, biomedical, and nanotechnologies.

## SUPPORTING MATERIAL

Supporting material can be found online at <https://doi.org/10.1016/j.bpr.2021.100007>.

## AUTHOR CONTRIBUTIONS

A.G. conceived and planned this study, designed and prepared the materials, performed experiments, and analyzed data. N.D.-K., S.Y., and Z.S. performed electrophysiology experiments and analyzed data. N.D.-K. and Z.S. planned, designed, and performed the biological aspects. S.W. designed and planned this study. All coauthors participated in writing the manuscript.

## ACKNOWLEDGMENTS

We thank Professor Dan Oron and Dr. Miri Kazes help with quantum yield measurements and for helpful discussions and Eugene Brozgol and Professor Yuval Garini for help with lifetime measurements.

This work has received funding from the European Research Council under the European Union's Horizon 2020 research and innovation program under grant agreement number 669941, by the Human Frontier Science Program research grant RGP0061/2015, by the BER program of the Department of Energy Office of Science grant DE-SC0020338, by the STROBE National Science Foundation Science &

Technology Center grant number DMR-1548924, by the Israel Science Foundation grant 813/19, and by the Bar-Ilan Research & Development Co., the Israel Innovation Authority, grant number 63392.

## REFERENCES

1. Yuste, R. 2015. From the neuron doctrine to neural networks. *Nat. Rev. Neurosci.* 16:487–497.
2. Nusser, Z. 2009. Variability in the subcellular distribution of ion channels increases neuronal diversity. *Trends Neurosci.* 32:267–274.
3. Miller, E. W. 2016. Small molecule fluorescent voltage indicators for studying membrane potential. *Curr. Opin. Chem. Biol.* 33:74–80.
4. Yan, P., C. D. Acker, and L. M. Loew. 2018. Tethered bichromophoric fluorophore quencher voltage sensitive dyes. *ACS Sens.* 3:2621–2628.
5. Yang, H. H., and F. St-Pierre. 2016. Genetically encoded voltage indicators: opportunities and challenges. *J. Neurosci.* 36:9977–9989.
6. Lin, M. Z., and M. J. Schnitzer. 2016. Genetically encoded indicators of neuronal activity. *Nat. Neurosci.* 19:1142–1153.
7. Chien, M.-P., D. Brinks, ..., A. E. Cohen. 2021. Photoactivated voltage imaging in tissue with an archaerhodopsin-derived reporter. *Sci. Adv.* 7:eabe3216.
8. Huang, Y.-L., A. S. Walker, and E. W. Miller. 2015. A photostable silicon rhodamine platform for optical voltage sensing. *J. Am. Chem. Soc.* 137:10767–10776.
9. Kulkarni, R. U., M. Vandenberghe, ..., E. W. Miller. 2018. *In vivo* two-photon voltage imaging with sulfonated rhodamine dyes. *ACS Cent. Sci.* 4:1371–1378.
10. Lazzari-Dean, J. R., A. M. M. Gest, and E. W. Miller. 2019. Optical estimation of absolute membrane potential using fluorescence lifetime imaging. *eLife.* 8:e44522.
11. Storace, D. A., L. B. Cohen, and Y. Choi. 2019. Using genetically encoded voltage indicators (GEVIs) to study the input-output transformation of the mammalian olfactory bulb. *Front. Cell. Neurosci.* 13:342.
12. Adam, Y., J. J. Kim, ..., A. E. Cohen. 2019. Voltage imaging and optogenetics reveal behaviour-dependent changes in hippocampal dynamics. *Nature.* 569:413–417.
13. Sundukova, M., E. Prifti, ..., P. A. Heppenstall. 2019. A chemogenetic approach for the optical monitoring of voltage in neurons. *Angew. Chem. Int. Ed. Engl.* 58:2341–2344.
14. Grenier, V., B. R. Daws, ..., E. W. Miller. 2019. Spying on neuronal membrane potential with genetically targetable voltage indicators. *J. Am. Chem. Soc.* 141:1349–1358.
15. Abdelfattah, A. S., T. Kawashima, ..., E. R. Schreiter. 2019. Bright and photostable chemigenetic indicators for extended *in vivo* voltage imaging. *Science.* 365:699–704.
16. Hernández-Juárez, C., R. Flores-Cruz, and A. Jiménez-Sánchez. 2021. Fluorescent probe for early mitochondrial voltage dynamics. *Chem. Commun. (Camb.)* 57:5526–5529.
17. Sepehri Rad, M., L. B. Cohen, ..., B. J. Baker. 2018. Monitoring voltage fluctuations of intracellular membranes. *Sci. Rep.* 8:6911.
18. Matamala, E., C. Castillo, ..., S. E. Brauchi. 2021. Imaging the electrical activity of organelles in living cells. *Commun. Biol.* 4:389.
19. Kulkarni, R. U., and E. W. Miller. 2017. Voltage imaging: pitfalls and potential. *Biochemistry.* 56:5171–5177.
20. Nag, O. K., M. E. Muroski, ..., J. B. Delehanty. 2020. Nanoparticle-mediated visualization and control of cellular membrane potential: strategies, progress, and remaining issues. *ACS Nano.* 14:2659–2677.

21. Ludwig, A., P. Serna, ..., A. Triller. 2020. Development of lipid-coated semiconductor nanosensors for recording of membrane potential in neurons. *ACS Photonics*. 7:1141–1152.
22. Denisov, I. G., and S. G. Sligar. 2017. Nanodiscs in membrane biochemistry and biophysics. *Chem. Rev.* 117:4669–4713.
23. Bradley, J., R. Luo, ..., D. A. DiGregorio. 2009. Submillisecond optical reporting of membrane potential in situ using a neuronal tracer dye. *J. Neurosci.* 29:9197–9209.
24. McGuire, H., M. R. Arousseau, ..., R. Blunck. 2012. Automating single subunit counting of membrane proteins in mammalian cells. *J. Biol. Chem.* 287:35912–35921.
25. Dubacheva, G. V., C. Araya-Callis, ..., R. P. Richter. 2017. Controlling multivalent binding through surface chemistry: model study on streptavidin. *J. Am. Chem. Soc.* 139:4157–4167.
26. Spinke, J., M. Liley, ..., W. Knoll. 1993. Molecular recognition at self-assembled monolayers: optimization of surface functionalization. *J. Chem. Phys.* 99:7012–7019.
27. Wu, Y., G. P. Lopez, ..., T. Buranda. 2007. Spectroscopic characterization of streptavidin functionalized quantum dots. *Anal. Biochem.* 364:193–203.
28. Szabó, Á., T. Szendi-Szalmáry, ..., P. Nagy. 2018. The effect of fluorophore conjugation on antibody affinity and the photophysical properties of dyes. *Biophys. J.* 114:688–700.
29. Chanda, B., O. K. Asamoah, ..., F. Bezanilla. 2005. Gating charge displacement in voltage-gated ion channels involves limited transmembrane movement. *Nature*. 436:852–856.
30. Nusser, Z., J. D. Roberts, ..., P. Somogyi. 1995. Relative densities of synaptic and extrasynaptic GABAA receptors on cerebellar granule cells as determined by a quantitative immunogold method. *J. Neurosci.* 15:2948–2960.
31. Nusser, Z., W. Sieghart, and P. Somogyi. 1998. Segregation of different GABAA receptors to synaptic and extrasynaptic membranes of cerebellar granule cells. *J. Neurosci.* 18:1693–1703.
32. Somogyi, P., J. M. Fritschy, ..., W. Sieghart. 1996. The gamma 2 subunit of the GABAA receptor is concentrated in synaptic junctions containing the alpha 1 and beta 2/3 subunits in hippocampus, cerebellum and globus pallidus. *Neuropharmacology*. 35:1425–1444.
33. Eugène, E., C. Depienne, ..., J. C. Poncer. 2007. GABA(A) receptor  $\gamma$  2 subunit mutations linked to human epileptic syndromes differentially affect phasic and tonic inhibition. *J. Neurosci.* 27:14108–14116.
34. Sassoè-Pognetto, M., P. Panzanelli, ..., J. M. Fritschy. 2000. Colocalization of multiple GABA(A) receptor subtypes with gephyrin at postsynaptic sites. *J. Comp. Neurol.* 420:481–498.
35. Shapira, Z., N. Degani-Katzav, ..., S. Weiss. 2021. Optical probing of local membrane potential with fluorescent polystyrene beads. *bioRxiv* <https://doi.org/10.1101/2021.04.21.440831>.
36. van der Velde, J. H. M., J. J. Uusitalo, ..., T. Cordes. 2015. Intramolecular photostabilization via triplet-state quenching: design principles to make organic fluorophores “self-healing”. *Faraday Discuss.* 184:221–235.
37. Buettner, G. R. 1993. The pecking order of free radicals and antioxidants: lipid peroxidation,  $\alpha$ -tocopherol, and ascorbate. *Arch. Biochem. Biophys.* 300:535–543.